THE JOURNAL OF PHYSICAL CHEMISTRY B

Article

Cite This: J. Phys. Chem. B 2019, 123, 2513−2524

pubs.acs.org/JPCB

Polydopamine Nanoparticles Prepared Using Redox-Active Transition Metals

Mikko Salomäki,*[,†,§] Tuomo Ouvinen,[†,∥] Lauri Marttila,[†,∥] Henri Kivelä,[†,§] Jarkko Leiro,[‡] Ermei Mäkilä,[‡,∥] and Jukka Lukkari*[,†,§]

[†]Department of Chemistry, [‡]Department of Physics and Astronomy, [§]Turku University Centre for Surfaces and Materials (MatSurf), and [∥]Doctoral Programme in Physical and Chemical Sciences, University of Turku, FI-20014 Turku, Finland

Supporting Information

ABSTRACT: Autoxidation of dopamine to polydopamine by dissolved oxygen is a slow process that requires highly alkaline conditions. Polydopamine can be formed rapidly also in mildly acidic and neutral solutions by using redox-active transition-metal ions. We present a comparative study of polydopamine nanoparticles formed by autoxidation and aerobic or anaerobic oxidation in the presence of Ce(IV), Fe(III), Cu(II), and Mn(VII). The UV−vis spectra of the purified nanoparticles are similar, and dopaminechrome is an early intermediate species. At low pH, Cu(II) requires the presence of oxygen and chloride ions to produce polydopamine at a reasonable rate. The changes in dispersibility and surface charge take place at around pH 4, which indicates the presence of ionizable groups, especially carboxylic acids, on their surface. X-ray photoelectron spectroscopy shows the presence of three different classes of carbons, and the carbonyl/carboxylate carbons amount to 5−15 atom %. The N 1s spectra show the presence of protonated free amino groups, suggesting that these groups may interact with the π-electrons of the intact aromatic dihydroxyindole moieties, especially in the metal-induced samples. The autoxidized and Mn(VII)-induced samples do not contain metals, but the metal content is 1−2 atom % in samples prepared with Ce(IV) or Cu(II), and ca. 20 atom % in polydopamine prepared in the presence of Fe(III). These differences in the metal content can be explained by the oxidation and complexation properties of the metals using the general model developed. In addition, the nitrogen content is lower in the metal-induced samples. All of the metal oxidants studied can be used to rapidly prepare polydopamine at room temperature, but the possible influence of the metal content and nitrogen loss should be taken into account.

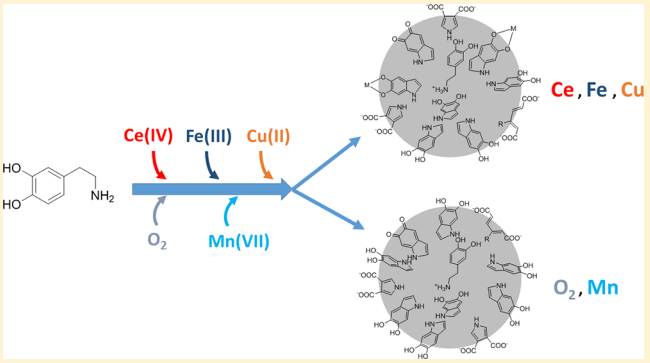

INTRODUCTION

Melanins are heterogeneous polymeric pigment materials formed from natural phenolic substances, either naturally or synthetically, and can be roughly classified into several large diverse groups: eumelanin, pheomelanin (containing sulfur) and neuromelanin (mixture of eumelanin and pheomelanin) in animals, and nitrogen-free allomelanin and pyomelanin in plants, fungi, and bacteria.[1−3] Eumelanin is the most studied of these, and has drawn much attention in materials science due to its versatile chemical and physical properties.[4−6]

Eumelanin biosynthesis, melanogenesis, uses mainly the amino acid tyrosine and the neurotransmitters dopamine (DA) and L-3,4-dihydroxyphenylalanine as reactants, and takes place in the melanosomes, which provide a matrix for the enzymatic reaction.[7] A synthetic alternative, polydopamine, can be obtained by a chemical oxidation of dopamine, and its properties are practically indistinguishable from those of the natural eumelanin. They are both nontoxic biodegradable semiconducting materials, which allow chemical modification, effectively bind many metals, scavenge free radicals, and convert practically all absorbed light into heat. The suggested applications for melanin or polydopamine include their use as e-ink,[8] and in energy storage and harvesting,[9−11] heavy-metal binding,[12] radical scavenging and irradiation protection,[13−15] structural coloration,[16] catalysis,[17] and various biomedical applications, including bioimaging, bioanalysis, drug delivery, and photothermal therapy.[18,19]

Melanins and polydopamine can be regarded as mixtures of oligomeric species and display structural and redox disorder.[20] The molecular structures of these materials are still debated.[18,21−23] The 5,6-dihydroxyindole (DHI) unit and its derivatives, both in catecholic and quinonoid forms, are the basic building blocks but incorporated pyrrolecarboxylic acids and dopamine molecules have been proposed and supported by experimental evidence. The building blocks are covalently linked to short oligomers or bound together noncovalently via $\pi-\pi$ interactions and hydrogen bonding.[24,25] A recent study suggests that the cation−π interactions between the proto-

Received: December 13, 2018
Revised: February 27, 2019
Published: February 28, 2019

DOI: 10.1021/acs.jpcb.8b11994
J. Phys. Chem. B 2019, 123, 2513−2524

nated free amino groups and the aromatic ring system of the DHI moieties play an important role.[26] Tetrameric porphyrin-like DHI units have been suggested as important structural components but have not been detected in polydopamine.[27−29] On the other hand, a recent study implies the formation of linear oligomers, and studies of carbonized nanoparticles (NPs) suggest a partially ordered supramolecular structure.[30,31] In spite of the controversial structure of the final material, the initial reaction steps in polydopamine formation are well known (Scheme 1) and consist of a six-electron

Scheme 1. Polydopamine Formation Pathway

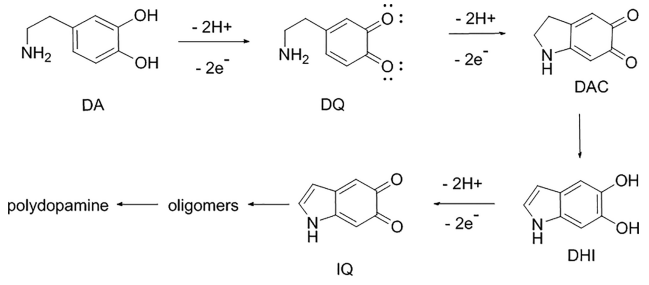

oxidation pathway from dopamine to dopaminequinone (DQ), dopaminechrome (DAC), 5,6-dihydroxyindole (DHI), and indolequinone (IQ). Further coupling and oxidation reactions lead to the final product.

Natural eumelanin and synthetic polydopamine generally aggregate during their formation to water-dispersible nanoparticles, but various additives in solution can enhance, delay, and modify the aggregation or even hinder the polymerization.[32,33] Autoxidation of dopamine in alkaline aqueous solutions is a standard method for polydopamine formation.[34] Nanoparticles are formed in the solution, and a thin film of the material is formed on practically any surface in contact with it. Site-specific deposition of nanoparticles has been achieved by surface-immobilized enzymes.[35] On the other hand, a protein matrix has been used to control polydopamine formation in a biomimic way,[36,37] and polyelectrolytes to adjust the nanoparticle size.[38] The autoxidation of dopamine by dioxygen is, however, a quite slow process and requires alkaline conditions, and other oxidants have also been used. We have recently studied the initial triggering phases in the dopamine oxidation and intramolecular ring closure and shown that pH 5 is the practical lower limit of autoxidation, although the reaction proceeds at a reasonable rate only at a much higher pH.[39] On the other hand, redox-active transition-metal ions allow fast polydopamine formation at considerably lower pH, in mildly acidic solutions. The autoxidation of dopamine has been reported to take place even at pH 1.5 under hydrothermal conditions, which can be attributed to the changes in the dielectric properties of water and the specific features of the reaction thermodynamics.[39,40] The use of ammonium persulfate, sodium periodate, or potassium chlorate as oxidants also allows polydopamine formation in weakly acidic and neutral solutions.[41,42] Metal ions are known to enhance dopamine oxidation, but there are very few comparative studies on the effect of different oxidants. If the autoxidation of dopamine is carried out in the presence of various nonoxidizing metal ions (Na^+, Ca^{2+}, Mg^{2+}, Co^{2+}), the nanoparticle formation and their properties are affected.[43] Fentonlike chemistry using a mixture of Fe(II) and hydrogen peroxide leads to a rapid generation of polydopamine nanoparticles.[44] On the other hand, oxidation of dopamine by Cu(II) under anaerobic conditions is a very slow reaction.[39,42,45,46] Oxidation by copper(II) produces thicker films than autoxidation, the nanoparticles are smaller, and their point of zero charge is shifted toward higher pH.[42,45,46]

We report here a comparative study of the effect of oxidants on the formation and properties of polydopamine nanoparticles. We have used three different kinds of oxidants. First, dissolved dioxygen is a two-electron oxidant, but its redox reactions with organic molecules are generally spin-forbidden, which leads to two sequential one-electron steps with a slow initial phase.[39,47,48] The autoxidation reaction produces highly reactive oxygen radicals, which can attack the material, and decomposition due to splitting of the catechol moiety has been observed in natural and synthetic melanin.[49,50] The autoxidized polydopamine nanoparticles serve as reference material in this work. Second, redox-active transition-metal ions Ce(IV), Fe(III), and Cu(II) are strong one-electron oxidants, and the mechanism of dopamine oxidation involves metal−catecholate complexes in this case. The oxidations have been carried out both in the absence and presence of dissolved oxygen, but the pH was set so low (4.5) that direct autoxidation was negligible. Cu(II) differs from the other metals because it forms the redox-active site of the redox enzymes involved in melanogenesis (e.g., catechol oxidase) and it actually becomes a better oxidant than Ce(IV) or Fe(III) at biological pH.[39,51] In addition, the thermodynamic stability range of Cu(I) is very narrow, and Cu(II) may act as a two-electron oxidant.[52] Finally, some experiments were done using Mn(VII), a three-electron oxidant, which is present as the permanganate anion in aqueous solution, and the mechanism of its reaction with dopamine most probably resembles that of the periodate ion.[53] The oxidizing power of the oxidants used varies considerably and is also pH-dependent. The formal redox potentials of the dioxygen/superoxide/peroxide, dopamine/dopamine semiquinone (DSQ)/dopaminequinone, Ce(IV)/Ce(III), Fe(III)/Fe(II), Cu(II)/Cu(I), and Mn(VII)/Mn(IV) redox pairs are shown in Table 1 under the nanoparticle synthesis conditions.[39,52] In addition, adding chloride ions in the solution makes Cu(II) a stronger oxidant, and in 0.1 M Cl^- solution, the formal potential of the Cu(II)/Cu(I) pair is +0.53 V.[39] Therefore, compared to other oxidants, molecular oxygen is a poor oxidant in all cases, and the effect of direct autoxidation in aerobic metal-induced dopamine oxidation can be assumed to be negligible. The nanoparticles formed are

Table 1. Formal Redox Potentials of the Oxidants Used

redox pair	DQH_2/DSQ[b]	DSQ/DQ[b]	$O_2/HO_2^{\bullet}$	$HO_2^{\bullet}/HO_2^-$	Ce(IV)/Ce(III)	Fe(III)/Fe(I)	Cu(II)/Cu(I)	Mn(VII)/Mn(IV)
$E^{\theta\prime}$ (V vs NHE)[a]	+0.31[c]	+0.15[c]	−0.20[c]	+0.68[c]				
	+0.80[d]	+0.17[d]	−0.17[d]	+1.18[d]	+0.62[d]	+0.41[d]	+0.24[d]	+1.3[d]

[a]Formal redox potential vs normal hydrogen electrode (NHE). [b]DQH_2 = dopamine, DSQ = dopamine semiquinone, DQ = dopaminequinone. [c]pH 9 (autoxidation). [d]pH 4.5.

DOI: 10.1021/acs.jpcb.8b11994
J. Phys. Chem. B 2019, 123, 2513−2524

thoroughly purified through dialysis and characterized using UV−vis spectroscopy, the measurement of size and surface charge, and X-ray photoelectron spectroscopy (XPS). Except for the copper-induced formation of polydopamine,[46] this is, to our knowledge, the first comparative study of polydopamine prepared using several redox-active transition metals, and it supplements our previous work on the initial stages of dopamine oxidation.[39]

EXPERIMENTAL SECTION

Materials. Dopamine hydrochloride, cerium(IV) ammonium nitrate, iron(III) chloride, poly(diallyl dimethylammonium chloride) (abbr. PDADMA, M_w = 100−200 kDa, 20% aqueous solution) (all from Sigma-Aldrich), $KMnO_4$ (Merck), and copper(II) sulfate pentahydrate (Merck) were used as received. All solutions were prepared in water distilled twice in quartz vessels. Silicon (111) wafers (Okmetic, Finland) were cleaned for 30 min in a fresh Piranha solution (3:1 conc. sulfuric acid and 30% hydrogen peroxide; Warning: Piranha solution is extremely corrosive and should not be stored in tightly closed vessels), rinsed with water, and dried at 110 °C.

Synthesis of Polydopamine Nanoparticles (NPs). Polydopamine nanoparticles were prepared using dissolved oxygen only and Ce(IV), Fe(III), Cu(II), or Mn(VII) salts with or without dissolved oxygen. For oxidation with dissolved oxygen only (autoxidized NPs), the pH of the dopamine hydrochloride solution (typically 0.2 mmol in 20 mL of water) was adjusted with 1 M NaOH to ca. 9, and the reaction was carried out at 50 °C under sonication (Hielscher UP100H tip sonicator) for 17 h.[54] Sonication was used to prevent precipitation of large particulates during the reaction and to produce nanoparticles of similar size as with metal-induced oxidation. The samples with metal ions were prepared at pH 4.5 at room temperature with a 6:1 (XPS) or equimolar (solution studies) metal/dopamine ratio. For the polydopamine formation in the absence of dissolved oxygen, the metal-ion and dopamine solutions were thoroughly deaerated with nitrogen and the reaction was carried under nitrogen atmosphere. The samples with dissolved oxygen were prepared in stirred open vessels. The reaction time depended on the sample but was ca. 4−5 h except in the case of Cu(II) with chloride (chloride concentration 300× that of dopamine) and/or dissolved oxygen, which were allowed to react for ca. 20 h. After reaction, the samples were dialyzed using a 3500 molecular weight cutoff membrane (Thermo Scientific Snake-Skin), first against dilute HCl solution (pH 4−4.5), followed by distilled water and, finally, dilute ammonia solution (pH 9−10) to solubilize as much of the material as possible. The aqueous polydopamine samples were stored at +4 °C.

Multilayer Formation. Polydopamine nanoparticles and PDADMA were sequentially adsorbed on the amino silanized walls of a flow-through cuvette or on a silanized silicon wafer and thoroughly rinsed with distilled water after every layer. The film on silicon was finally dried with a nitrogen flow. The PDADMA solution concentration was 10 mM with respect to the monomer and contained 0.1 M NaCl.

Characterization. For XPS measurements, the silicon wafers were thermally coated with gold with a chromium adhesive layer (Edwards E306A). The metal films were cleaned with oxygen plasma (Harrick plasma cleaner and PlasmaFlo PDC-FMG), and a few drops of polydopamine suspension were added and allowed to evaporate in vacuum at room temperature. The suspensions were sonicated in an ultrasonic bath to disperse polydopamine particles when necessary. X-ray photoelectron spectra were recorded on a PerkinElmer 5400 small-spot ESCA spectrometer using twin anode with Mg Kα radiation and the takeoff angle of 45°, and the spectra were analyzed using the Unifit 2013 fitting program (Unifit Scientific Software GmbH, Leipzig, Germany). Atomic force microscopy (AFM) images were recorded using a diCaliber atomic force microscope (diCaliber, Bruker) in a tapping mode. Scanning electron microscopy (SEM) imaging was also carried out with some samples (see Supporting Information for details).

Aliquots of dialyzed NP suspensions were added to buffers of different pH values, and the particle size and ζ potential were measured using dynamic and electrophoretic light scattering (Malvern Zetasizer Nano ZS). UV−vis spectra of similarly prepared suspensions at different pH values were measured (Cary 60 UV−vis spectrophotometer, Agilent Technologies) before and after centrifugation for 10 min at 50 000g (Heraeus Biofuge Stratos table top centrifuge). The ratio of the absorbances at 300 nm was used as a measure of the nanoparticle dispersibility.

RESULTS AND DISCUSSION

Nanoparticle Formation. The autoxidation of dopamine by dissolved oxygen was carried out at elevated temperature at pH 9 to speed up the slow reaction. From our previous studies, we know that the UV−vis spectra taken during the polydopamine formation show the reaction to initially proceed via the formation of leucodopaminechrome and dopaminechrome (maxima at ca. 285 and 480 nm, respectively).[39] Later, the spectrum begins to resemble the typical featureless polydopamine/melanin spectrum but there is a clear maximum at ca. 275 nm and a shoulder at ca. 350 nm. Similarly, with low concentrations of Ce(IV) or Fe(III) and dopamine at pH 4.5, in the absence of oxygen, dopaminechrome was initially formed (480 nm) while absorbance decreased below 400 nm. Cu(II) alone is a very weak oxidant at this pH, but the addition of chloride ion increases its redox potential and facilitates the reaction.[39] The absorbance increases between 300 and 600 nm, both with and without oxygen, showing that dopaminechrome is initially formed also in this case. When redox-inactive metal ions were present during the autoxidation, the spectra always showed the presence of dopaminechrome (shoulder at 480 nm), but other peaks appeared at ca. 410 nm (Na^+, Ca^{2+}) or 580−600 nm (Mg^{2+}, Co^{2+}).[43] The authors attributed these peaks to dopaminequinone (maximum at 395 nm)[50] and a dihydroxyindole dimer. Dopaminechrome (480 nm) was also observed during oxidation with ammonium peroxodisulfate and sodium periodate.[42] Therefore, the major intermediate species during the early stages of the polydopamine formation is dopaminechrome in all cases.

With higher oxidant and dopamine concentration, the solution rapidly turned deep dark in most cases. With transition-metal ions, the synthesis was carried out at pH 4.5 in the presence and absence of dissolved oxygen. In all cases, a dark solution was obtained, but the anaerobic Cu(II)-dopamine sample darkened significantly only during the dialysis when the pH increased to 6−7. This is in accordance with the previous results, which show that the onset pH is ca. 6 for the dopamine oxidation with Cu(II) in the presence of O_2(aq).[39] The reaction mixtures were thoroughly dialyzed to remove loosely bound small molecules and ions. All of the polydopamine samples prepared in the presence of transition

DOI: 10.1021/acs.jpcb.8b11994
J. Phys. Chem. B 2019, 123, 2513−2524

metals, with or without oxygen, displayed a typical, monotonously changing spectrum with a shoulder at ca. 260−300 nm (Figure 1). A peak at 280 nm has been observed

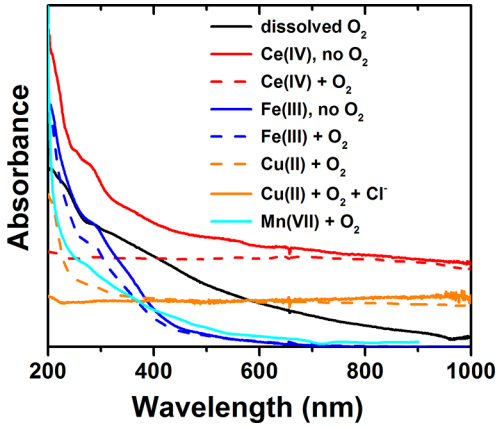

Figure 1. UV−vis spectra of dialyzed polydopamine samples (in basic solution). Note that the absorbance scale is arbitrary; the spectra of dilute samples have been multiplied for clarity.

in the spectra of Cu(II) oxidized polydopamine, too, with smaller shoulders at 360 and 420 nm.[46] In general, the metal-oxidized polydopamine samples display various peaks or shoulders in their spectrum because the material is formed in a partially oxidized state.[55] The nondialyzed samples of polydopamine (Figure S1), either autoxidized or prepared with Fe(III) and Cu(II), also displayed the 270−280 peak (or shoulder), but with Ce(IV), the peak was at lower wavelength, at ca. 250 nm, and the peaks are less pronounced. A definite identification of the species responsible for these spectral features is not possible because of the structural and redox heterogeneity of the solution. However, the peak at ca. 280 nm most probably belongs to dopamine, DHI, or similar species, and is markedly reduced when small molecules are rinsed away during the purification step (Figure S1).[39]

In general, the spectra obtained using Ce(IV) rather closely resemble the featureless spectra of autoxidized polydopamine, whereas the use of Fe(III) resulted in spectra with no absorbance above 700 nm (except before dialysis). This could be caused by effective iron-mediated bonding of smaller aggregates to larger ones. Finally, it should be noted that the use of Ce(IV) requires a high buffer capacity in the solution. With low buffer concentration, the pH rapidly rises from the initial 4.5 to ca. 7, probably due to the breakdown of the highly acidic Ce(IV) aqua complexes.

Nanoparticle Dispersions. The diameter of the nanoparticles in the dialyzed aqueous suspensions of the samples,

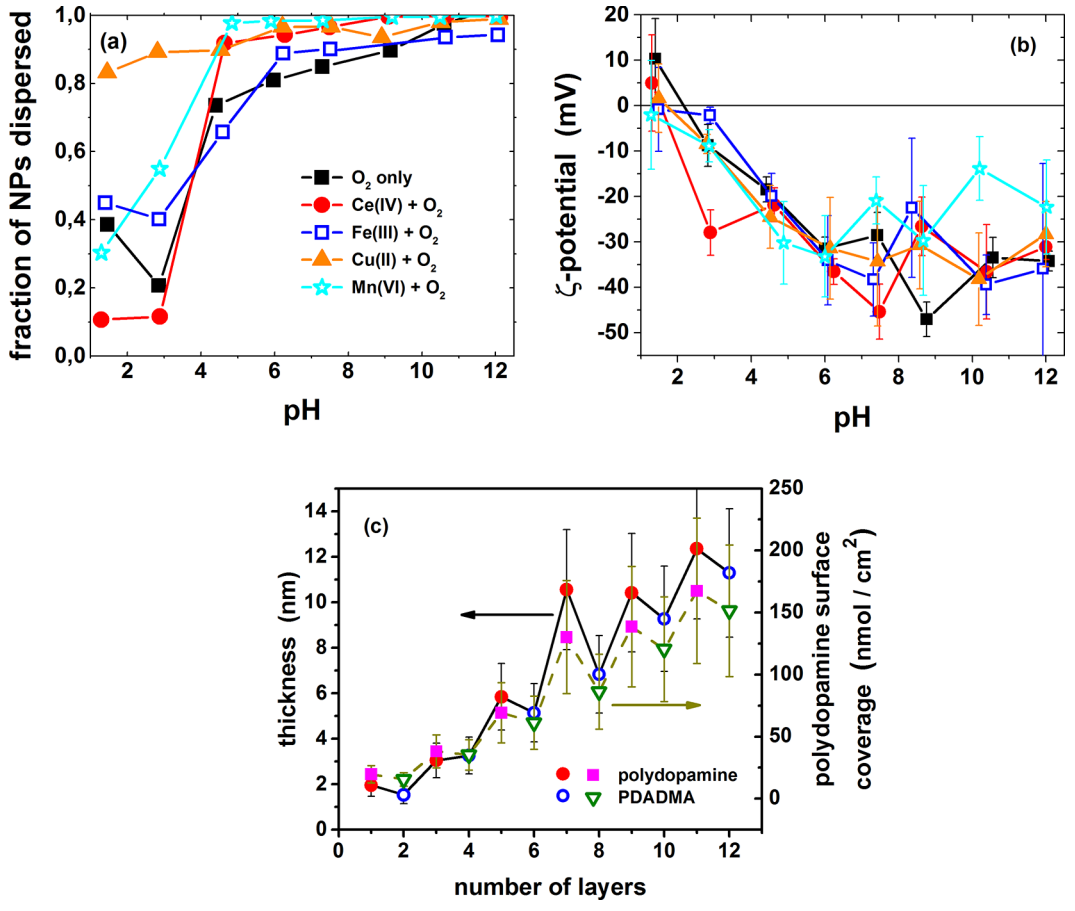

Figure 2. (a) Dispersibility of the differently prepared nanoparticles as a function of pH, measured by the ratio of the absorbance at 300 nm after and before centrifugation; (b) ζ potential of the nanoparticles as a function of pH (lines and symbols are the same in both (a) and (b)); lines are shown only as a guide to the eye, and the error bars correspond to standard deviations of the mean values from several measurements; (c) changes in the film thickness and polydopamine surface coverage (corresponding to a species $C_8NO_2H_4$; see ref 61) during the layer-by-layer (LbL) buildup of a polydopamine/PDADMA multilayer on one wall of a flow-through cuvette (the error bars based on accuracy given in original papers).

DOI: 10.1021/acs.jpcb.8b11994
J. Phys. Chem. B 2019, 123, 2513−2524

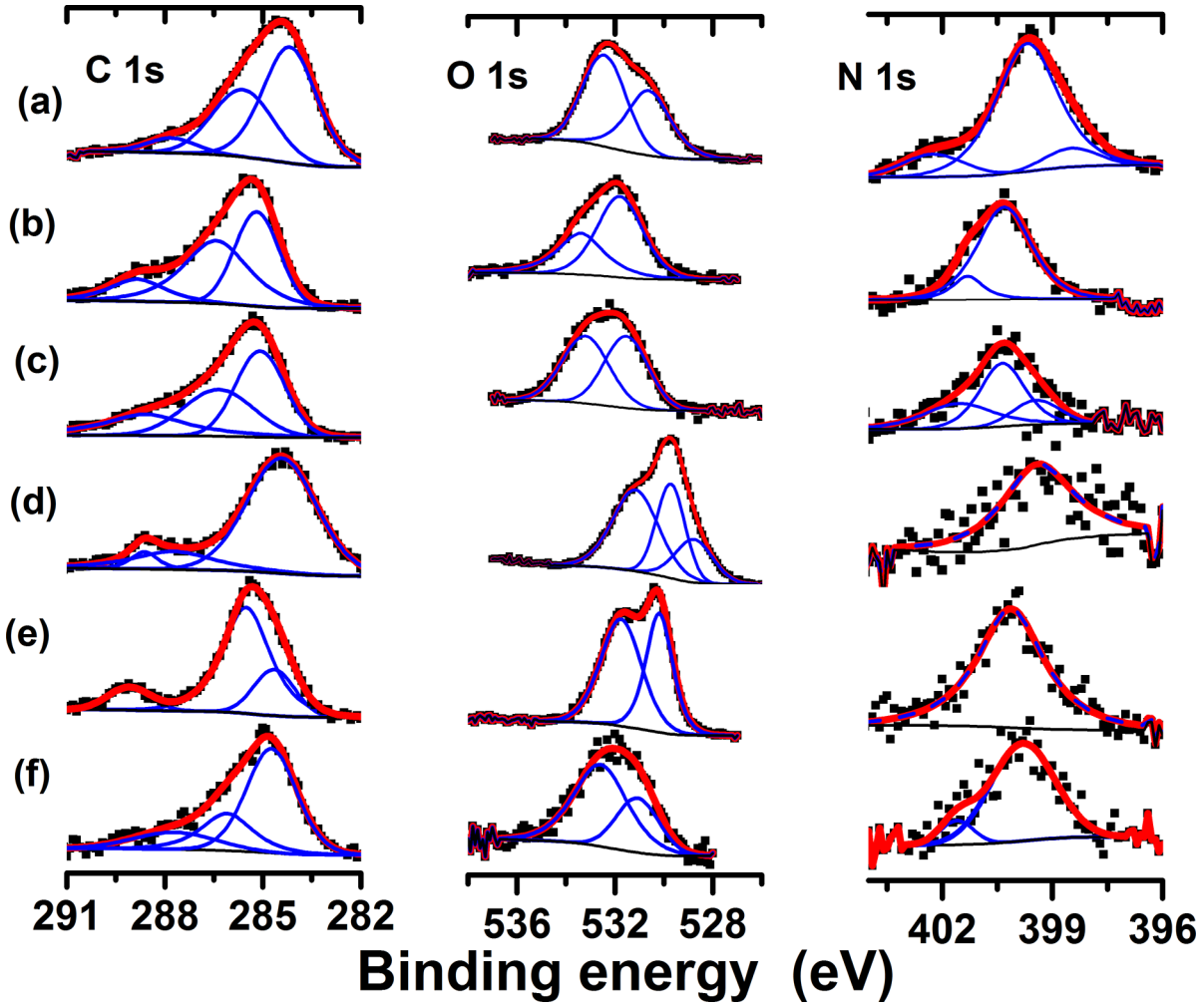

Figure 3. Deconvoluted XPS images of the C 1s, O 1s, and N 1s regions of polydopamine nanoparticles. Samples: (a) autoxidized (dissolved O_2); (b) Ce(IV) without O_2; (c) Ce(IV) and O_2; (d) Fe(III) without O_2; (e) Fe(III) and O_2; and (f) Cu(II) and O_2 with NaCl. The red line is the sum of the deconvoluted bands (blue lines); Shirley background is shown as a black line.

prepared in the presence of dissolved oxygen (including the autoxidized sample), was measured using laser scattering. In all cases, the *z*-average of the nanoparticle diameter was 105 ± 20 nm, in accordance with the AFM and SEM images (Figures S3 and S4), and is smaller than in the work discussing the effect of Cu(II).[46] The polydopamine nanoparticles tend to sedimentate from the solution at low pH (Figure S2), and we used the ratio of absorbance at 300 nm after and before centrifugation as a measure of the fraction of dispersible nanoparticles. The particle dispersibility exhibits a clear increase around pH 4 (Figure 2a). The dispersibility is connected to the surface charge (ζ potential) of the nanoparticles. In very acidic conditions (below pH 3), the ζ potential is generally positive or close to zero and turns negative at higher pH.[43,46] Incorporation of nonelectroactive metal ions has been reported to shift the point of zero charge downward by approximately one pH unit, and the authors attributed this to a higher amount of pyrrolecarboxylic acids, although without further justification.[43] On the other hand, copper has been reported to bring about an opposite and larger change.[46] With the nanoparticles prepared using the redox-active metal ions in this work, the ζ potential in acidic solutions was more negative than that of the purely autoxidized ones (Figure 2b). This also induced a small downward shift (less than 1 pH unit) in the isoelectric point, but, in all cases, there was a steep decrease of the surface charge in the pH range of 3−5, coinciding with the change in dispersibility, until it stabilized at a clearly negative value (−35 ± 10 mV) above pH 6. These observations are different from those reported previously for copper-oxidized polydopamine, but,[46] in our work, dissolved oxygen was always present, the copper concentration was lower, the reaction time was shorter, and, consequently, the nanoparticles were also considerably smaller. We assume that with the small nanoparticles, the surface effects are more dominant than with the larger ones. It should be pointed out that the dispersibility of the Cu(II)-based nanoparticles in Figure 2a seems exceptionally high at low pH, but it can be attributed to their very low concentration. The polydopamine formation with copper, even in the presence of oxygen, is so slow that large nanoparticles have not had time to form in the short reaction time used.[39]

The consistent changes in the observed dispersibility and ζ potential indicate the presence of ionizable groups on the nanoparticle surface. However, the local pH on the nanoparticle surface lags behind the bulk pH by the amount given by $\Delta pH = pH_{surface} - pH_{bulk} = 0.434F\phi/RT$, where ϕ, F, R, and T are the surface potential, Faraday constant, gas constant, and absolute temperature, respectively.[56] With fully ionized

DOI: 10.1021/acs.jpcb.8b11994
J. Phys. Chem. B 2019, 123, 2513−2524

Table 2. Composition of the Polydopamine Nanoparticles

oxidant[a]	Ce(IV)	Ce(IV) + O_2	Fe(III)	Fe(III) + O_2	Cu(II) + O_2 + Cl
metal atom %	1.3	2.4	17.4	20.0	1.3
redox ratio	Ce(III)/Ce(IV) = 1:1	Ce(III)/Ce(IV) = 2:3	Fe(II)/Fe(III) = 1:2	Fe(II)/Fe(III) = 2:3	Cu(0,I)/Cu(II) = 1:1
C/N/O	10.8:1:4.9	9.1:1:2.9	9.7:1:18.4	19.1:1:20.2	14.2:1:4.2

[a]For the autoxidized sample C/N/O ≈ 8.5:1:2.4.

nanoparticles with a ζ potential of ca. −35 mV, the surface pH is ca. 0.6 units lower than the bulk pH, and this effect widens the apparent ionization range around the pK_a of the surface species. The pK_a values of the hydroxyl groups of the catechol moiety in melanin are close to those in dopamine and will not influence the behavior except at high pH.[57] The pK_a value is ca. 4.7 in the dopamine semiquinone and 6.8 in the DHI semiquinone, which are not, however, stable in an aqueous environment.[39] Quinone imine tautomerization in the oxidized dihydroxyindole unit shifts the pK_a value to ca. 6, which coincides with the reported behavior of the ζ potential with larger copper-containing nanoparticles.[46,49] Carboxylic groups have not been observed in the IR spectra of polydopamine, possibly due to the broad intense absorption in that range, but the catechol moiety may undergo an oxidative intradiol cleavage, especially in the presence of transition metals, to yield muconic acid, and the decomposition of the DHI moiety during the oxidation has also been shown to produce pyrrole dicarboxylic acid.[49,50,58] The first pK_a value of muconic acid is in the approximate range of 3.0−4.5 and the second below 5, and these values are well in accordance with the range of the ζ potential and dispersibility changes observed.[59]

It is interesting to try to estimate the surface concentration of ionized groups in the nanoparticles using the functional dependence of the ζ potential to the effective surface charge (see Supporting Information for details).[60] The ionic strength of the nanoparticle solutions varies with pH, but the equations allow to estimate that the surface concentration of charged groups is ca. 1.75×10^{13} cm^{-2}. If we approximate polydopamine by poly-DHI and assume a bulk density of ca. 1.5 g cm^{-3}, then we can estimate that ca. 3% of the catechol moieties on the nanoparticle surface have been cleaved to dicarboxylic acids.[61] It should be noted that this estimate represents the lower limit of the cleaved catechols because it relies on the ζ potential, which is the potential on the shear plane. It is usually associated with the outer Helmholtz plane, where adsorbed ions shield part of the true surface charge. However, it is roughly in accordance with the atom % of C═O species (which includes also quinonoid species) found by XPS (vide infra). The ionized groups on the surface make nanoparticles polyanions and render them suitable for the polyelectrolyte layer-by-layer sequential assembly.[62] An example of the buildup of a polydopamine/PDADMA multilayer is shown in Figure 2c. The film thickness and polydopamine surface coverage were estimated from the spectral data using the mass and molar absorption coefficients reported in the literature.[61,62] The growth is clearly linear after two (polydopamine/PDADMA) bilayers, but the adsorption of PDADMA always leads to a significant removal of polydopamine from the surface. The multilayer films display a very rough globular morphology of small particles (diameter, ca. 100−200 nm) aggregated together to large boulders (Figure S4).

Nanoparticle Surface Chemistry. To gain information about the surface chemistry of the polydopamine nanoparticles and its sensitivity to the synthesis conditions (aerobic vs anaerobic, autoxidation vs metal-induced), we have measured the X-ray photoelectron spectra of the dried nanoparticle suspensions on evaporated gold surfaces. Because the electron attenuation length in organic material is only a few nanometers, much smaller than the average nanoparticle diameter, XPS gives information only of the surface region of the nanoparticles.[63] However, because the interactions with the environment take place via surfaces, this is the most important part of the particles. The autoxidized polydopamine serves as a reference sample in this case, too. When metals were used in the presence of oxygen, the pH was set so low (pH 4.5) that direct autoxidation of dopamine was negligible, although oxygen may participate in the reaction through other reaction paths (oxidation with Cu(II) in the presence of oxygen only yielded too dilute polydopamine dispersions for the XPS analysis).[39] The deconvoluted C 1s, O 1s, and N 1s spectra are shown in Figure 3, and the binding energies (BEs) of the bands in Table S2. In general, the differences between the samples were not very large (Table S2, Figures 3, and S5). The C/N/O ratio of the autoxidized polydopamine was 8.5:1.0:2.4 (C/O ≈ 3.5), which is close to the theoretical composition C_8NO_2 for poly-DHI or $(dopamine)_n$, but the nitrogen content was lower in other samples (Table 2). The C/O ratios of the Cu(II)- and Ce(IV)-induced samples were close to that of the autoxidized one (2.2−3.4), but the Fe(III)-induced samples contained a large surplus of oxygen over carbon. The reduced nitrogen content suggests removal of species with a high nitrogen content during the reaction with metal oxidants, which would also lead to relatively low signal-to-noise (S/N) ratios in the N 1s spectra. Transition metals enhance the intra- and extradiol cleavage of the catechol ring under aerobic conditions and form cyclic intermediates, which hydrolyze in water and produce smaller molecules.[64,65] The catechol ring cleavage is much more common than that of the pyrrole moiety, and small nitrogen-containing species (e.g., pyrrole di- and tricarboxylic acids) probably form as the result of the diol cleavage. This also disrupts the supramolecular structure of the material, affects the intermolecular interactions, and allows small molecules (with higher N/C ratios than in poly-DHI) to leak out of the material. On the other hand, the very high oxygen content of the iron-induced samples can be explained by aqua complex formation (vide infra).

We have previously noted that the binding energies reported for various carbon and oxygen species in melanin-type materials may differ considerably (a compilation of the literature data is given in Table S1 in the Supporting Information).[55] However, the binding energy differences between various assigned species are more consistent and allow to recognize different classes of atoms in chemically specified environments. In all of the cases studied in this work, the C 1s spectrum can be deconvoluted using three peaks. We attribute the peak at the lowest binding energy (284−285.5 eV) to C−H, aromatic and adventitious carbon, and the peak at 285.5−287.5 eV to carbon bonded to nitrogen or a hydroxyl

DOI: 10.1021/acs.jpcb.8b11994
J. Phys. Chem. B 2019, 123, 2513−2524

group.[21,55,66−71] All spectra showed a small fraction (ca. 5−15 atom %) of oxidized carbon with a binding energy of 287.5−289.0 eV, which is assigned to a carbonyl carbon. The C═O carbon in a carboxylic acid group has a higher binding energy than the carbon in the quinone form of the catecholate moiety, but their deconvolution was not reliable. Sodium ions bound to carboxylate groups increase the C 1s binding energy, and they are present in polydopamine formed by oxidation with the NaCl-containing Cu(II) solutions, in spite of the thorough sample purification because a small but unambiguous Na 1s signal (at 1071.5 eV, corresponding to a Na salt; Figure S5) was seen in the spectra, but no Cl 2p signal was observed.[9] The O 1s spectra are simpler and exhibit two peaks in most cases, with the high BE component at ca. 532−533 eV being assigned to C−O and the low BE component at ca. 530.5−531.5 eV to C═O.[16,21,55,66−69,72] In the sample prepared using Fe(III) in the absence of oxygen, the O 1s signal could be divided into three peaks. The peak at the lowest binding energy corresponds to an iron oxide, the position of which does not depend in any straightforward way on the oxidation state of iron.[73] The iron oxides are artifacts formed from hydroxides in the dehydrated XPS sample. The second peak (529.7 eV) is assigned to Fe−O−C, i.e., an iron catecholate.[74] The peak with the highest BE (531.2 eV) represents C═O, which shows that all of the catechol moieties in the nanoparticle surface region are either oxidized or complexed to iron. The nanoparticles prepared aerobically in the presence of Fe(III) display only the catecholate and carboxyl species (a very small contribution of iron oxide, ca. 1−2%, may be included) for reasons not clear at the moment.

The N 1s spectrum of the autoxidized sample is very similar to that recently reported showing three different nitrogen species.[26] In general, a pyridinic or aromatic nitrogen (nitrogen with a lone electron pair, C═N) has a binding energy of ca. 398.3 eV, a pyrrolic nitrogen (nitrogen in a five-membered ring, C−N−C) ca. 400.1 eV, a graphitic (quaternary) nitrogen ca. 401.4 eV, and a protonated amino nitrogen ($R-NH_3^+$) ca. 401−402 eV,[26,75−78] and these values are generally in accordance with those reported for melanin-type materials (Table S1).[16,21,55,66−70,79,80] Uncyclized dopamine molecules have been reported in polydopamine, and their signature would be a band corresponding to an amino nitrogen. Free unprotonated amines usually have a binding energy of ca. 399.5 eV, overlapping that of the pyrrolic nitrogen (secondary amine), which makes their unambiguous spectral deconvolution difficult.[26,77] However, based on the microscopic pK_a values of dopamine, the effective macroscopic pK_a value for the amino group in dopamine is ca. 10, and a large fraction of the free amino groups is protonated under normal reaction and XPS sample preparation conditions.[39] Therefore, the major peak at ca. 400 eV in the N 1s spectra of all our nanoparticles is assigned mainly to the pyrrolic nitrogen in the intact DHI moieties. A smaller peak was observed at ca. 401−402 eV in all samples, except those prepared in the presence of Fe(III), which can be attributed to protonated amino groups. A band in this BE range has been observed also in most studies of autoxidized polydopamine.[26,67−70,72] A small signal (below 10%) at 398.5 eV was observed in the autoxidized and the aerobic Ce(IV)-oxidized samples, suggesting a small amount of pyridinic nitrogen (C═N) in those nanoparticles. This and the protonated amino components are probably present also in the iron-oxidized samples, in which only one wide band assigned to pyrrolic nitrogen could be reliably deconvoluted. The assignment of the low-BE band to pyridinic nitrogen species is somewhat problematic, although they have often been reported in autoxidized polydopamine samples.[26,67,69,70,79] However, imine structures have also been ruled out based on XPS data[21] and theoretical calculations imply the instability (in the gas phase) of the DHI and IQ tautomers with C═N bonds with respect to other tautomeric forms.[81,82] On the other hand, the complexation of the catecholate with a metal may favor the imine form in a DHI structure (Scheme 2). The C═N band is always of quite low

Scheme 2. Metal-Induced Resonance

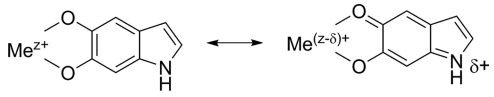

intensity, and we suggest that the major pyridinic contribution may be due to small degradation products still within the material. In fact, we have found some evidence for such molecules in the mass spectroscopic study of polydopamine and melanin.[55] Low-binding-energy nitrogen has also been associated with metal-bound nitrogen, but this is improbable because the metal-bonding site in melanin has been shown to be the catecholic moiety.[83]

In some cases, the whole C 1s and O 1s spectra and their deconvoluted component bands (Figure 3) display an upward shift in binding energy compared to the autoxidized sample. Shifts in the observed binding energy can be caused by sample charging or the use of different substrates. However, in this case, these effects can be ruled out as all of the samples consisted of thin nanoparticle aggregates on a gold surface, and the Au 4f signals were consistent within the instrumental error limits. Figure 3 shows that the largest shifts (ca. 1 eV) are observed in the Ce- and Fe-containing samples while the aerobically prepared Cu-containing samples are shifted by a smaller amount (less than 0.5 eV). Collective electrostatic effects have been shown to influence the appearance of the XPS spectra.[84,85] Recently, cation−π interactions between the protonated free amino group and the aromatic dihydroxyindole moiety have been shown to be important structural characteristics in polydopamine.[26] The N 1s spectra of the Ce- and Cu-containing samples show the presence of protonated amino groups at 401−402 eV (the S/N ratio of the Fe-containing samples is too low to allow reliable deconvolution, but the width of the N 1s band suggests more than one nitrogen species). We tentatively suggest that charged $-NH_3^+$ groups interacting with the aromatic π-electrons in the DHI moieties cause the observed positive shift of the C 1s and O 1s binding energies. The smaller effect observed with Cu-induced sample can be ascribed to the sodium ions in the synthesis solution, which tend to mask the effect of protonated amino groups.[26] On the other hand, the autoxidized sample also displays a band assigned to a protonated amino group. Therefore, we must further assume that the metal-induced polydopamines possess a more ordered supramolecular structure, where cation−π interactions have a stronger role. In fact, Cu(II) has previously been shown to produce polydopamine structurally different from the autoxidized material.[46] Favorable cation−π interaction should also lower the binding energy of the protonated amino nitrogen, which is, indeed, in accordance with the higher BE observed for the $-NH_3^+$ group in the autoxidized sample.

DOI: 10.1021/acs.jpcb.8b11994
J. Phys. Chem. B 2019, 123, 2513−2524

The factor that clearly differentiates the autoxidized and the Mn(VII)-induced samples from the others is the presence of metals in the latter ones (Table 2 and Figure S6). Metals Ce, Fe, and Cu were found in the final material, even after successive dialysis, which demonstrates the high complexing capability of polydopamine (however, we have not tested extraction with ethylenediaminetetraacetic acid or other effective ligands).[83] All of the metals were found in a mixture of various oxidation states, i.e., Ce(IV/III),[86,87] Fe(III/II),[73] and Cu(II/I/0),[88] but their ratios do not provide reliable information because the samples had been exposed to ambient atmosphere before insertion into the measurement chamber. In addition, the differentiation between Cu(I) and Cu(0) is very difficult and, for these reasons, the two-electron oxidation by Cu(II) cannot be excluded.[89] To estimate the effect of various factors on the metal content in polydopamine samples, we model the process by a redox reaction coupled to complexation reactions with DHI and any other ligand(s) X present (Scheme 3; X = OH, carboxylates etc.). We assume

Scheme 3. Schematic Model Used in the Semiquantitative Analysis of Metal Binding to Polydopamine (X = Any Nonelectroactive Innocent Ligand Present)[a]

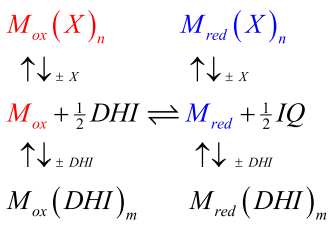

[a]Oxidized and reduced metal not bound to DHI in red and blue, respectively

that the reactions take place between individual DHI moieties, the metal ions, and various other possible ligands in a poly-DHI matrix. In addition, we assume that pH is low enough (pH below ca. 8) so that the deprotonation of the DHI hydroxyl groups needs not be taken into account.[90] Complex formation with indolequinone (IQ) and semiquinone concentration will also be neglected.

The gross chemical state of the system is defined by the oxidizing power of the metal and the complexation properties of its oxidized and reduced forms. These factors are described by three parameters. The relative extent of the redox reaction, $\xi = [M_{red}^{(tot)}]/M^{(tot)}$, where $M^{(tot)}$ and $M_{red}^{(tot)}$ are the total amount of metal and the total amount of its reduced form, respectively, is a monotonic sigmoidal function $\xi = \xi(\Delta\varepsilon)$ of the dimensionless potential difference variable $\Delta\varepsilon = 2F\Delta E^{\theta\prime}/RT$, which ranges from 0 to 1 (Figure S7). Here, $\Delta E^{\theta\prime} = E_M^{\theta\prime} - E_{IQ/DHI}^{\theta\prime}$ is the formal potential difference between the one-electron formal potential of the metal couple and the two-electron formal potential of the IQ/DHI pair. The formal redox potentials of the metals studied have been calculated in our earlier work,[39] and the formal potential of the IQ/DHI pair decreases by 60 mV per pH unit. For this pair, we use the measured value +0.73 V versus NHE for an autoxidized polydopamine film in 0.5 M H_2SO_4 (pH = 0.3).[91] The two other dimensionless variables, χ_{ox} and χ_{red}, are defined as

$$\chi_{ox,red} = \frac{\alpha_{ox,red}(DHI) - 1}{\alpha_{ox,red}(DHI) + \alpha_{ox,red}(X) - 1} \quad (1)$$

Here, the α factors are the side reaction coefficients of the oxidized and reduced metal ions for complexation with DHI or any other innocent and nonelectroactive ligand(s) X present.[39,92] The side reaction coefficients are given for any ligand L as $\alpha(L) = 1 + \sum_n \beta_n(L)[L]^n$, where $\beta_n(L)$ is the cumulative stability constant for the complex ML_n. The parameters χ also range from $\chi = 0$ (no complexation with DHI) to $\chi \sim 1$ (complexation with DHI much more important than with X). Assuming that all reactions are reversible and DHI is an innocent ligand, we can obtain an expression for the relative amount of metal bound to DHI (only mononuclear complexes) as a function of these three dimensionless variables (see Supporting Information for details)

$$\phi = [M(DHI)^{(tot)}]/[M^{(tot)}] = (1 - \xi)\chi_{ox} + \xi\chi_{red} \quad (2)$$

However, the variables are not independent because the side reaction coefficients $\alpha_{ox,red}(DHI)$ are given in terms of the free DHI concentration $[DHI^{(free)}]$, which depends on the extent of the reaction ξ and, therefore, the side reaction coefficients are functions of ξ. On the other hand, the concentration [X] of other ligands can be assumed constant. Now $[DHI^{(free)}]$ and $\alpha_{ox,red}(DHI)$ are monotonous functions of ξ so that $\alpha_{ox,red}(DHI) \to 1$ and $\chi_{ox,red} \to 0$ when $\xi \to 1$. This allows us to determine the limiting behavior of ϕ in various cases. First, if M_{ox} is a weak oxidant, then $\xi \sim 0$ and $\phi \approx \chi_{ox} = [\alpha_{ox}(DHI) - 1]/[\alpha_{ox}(DHI) + \alpha_{ox}(X) - 1]$. Metal binding is determined by the tendency of M_{ox} to bind DHI over other ligands present. This is the case with Cu(II) for which $\Delta\varepsilon \approx -19$ ($\xi \sim 0$, at pH 4.5). Second, if M_{ox} is a strong oxidant, then $\xi \sim 1$ and $\phi \approx 0$ because $\phi \approx \chi_{red} = [\alpha_{red}(DHI) - 1]/[\alpha_{red}(DHI) + \alpha_{red}(X) - 1] \sim 0$. A negligible amount of metal is bound to DHI as is the case for Ce(IV) with $\Delta\varepsilon \approx 11$ ($\xi \approx 0.97$, at pH 4.5). Third, if M_{ox} is a moderate oxidant, then $\phi = (1 - \xi)\chi_{ox} + \xi\chi_{red}$, and we have $0 < \xi < 1$ and $1 - \xi \sim \xi$. In this case, metal binding is controlled by χ_{ox} and χ_{red}, which are, in turn, determined by the relative tendencies of the oxidized and reduced metal to bind DHI over X. This is the case for Fe(III), which forms strong complexes with DHI and has $\Delta\varepsilon \approx -5$ ($\xi \approx 0.14$, at pH 4.5). Interestingly, Cu(II) in the presence of chloride is a stronger but still moderate oxidant with $\Delta\varepsilon \approx 4$ ($\xi \approx 0.78$). However, Fe(III) forms very stable catecholate complexes, and $\chi_{ox} \sim 1$ (X = OH and only 1:1 DHI complex) because at this pH, $\alpha_{Fe(III)}(DHI) \sim 10^{34}$–$10^{37}$ (for 1 mM DHI).[39,93] In addition, Fe(II) also complexes DHI and $\alpha_{Fe(II)}(DHI) \sim 10^8$ under the same conditions, making also $\chi_{red} \sim 1$ in this case.[94] This suggests a high iron content in the material. Cu(II) also forms strong catecholate complexes with $\alpha_{Cu(II)}(DHI) \sim 10^{18}$ and only weak hydroxo or chloro complexes, resulting in $\chi_{ox} \sim 1$ in this case.[39,95] Studies on copper-based enzymes and complexes suggest that Cu(I) does not form stable complexes with the hard catecholate ligand.[51,96] On the other hand, it forms stable chloro complexes (resulting in an increased oxidizing power in the presence of chloride), which means that χ_{red} is small for copper.[39] Therefore, the model predicts low copper content also in the presence of chloride. In this context, it may be interesting to note that the enzymes involved in melanogenesis use copper in their active sites, and increased levels of iron are found in neuromelanin in the substantia nigra in the case of brain aging and Parkinson's disease.[51,97]

The simple model presented can semiquantitatively rationalize the metal content in the polydopamine samples (Scheme

DOI: 10.1021/acs.jpcb.8b11994
J. Phys. Chem. B 2019, 123, 2513–2524

Scheme 4. Factors Affecting the Metal Content in Polydopamine

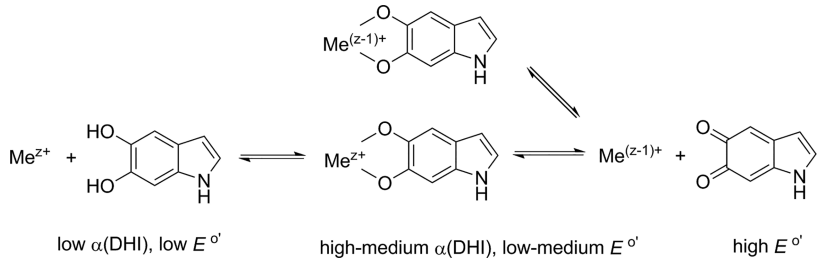

4) as its conclusions are in accordance with the observed metal contents. In nanoparticles prepared using cerium and copper, the metal content was small, in the range of 1−2.5 atom %, in accordance with previous studies of material oxidized in the presence of alkali or alkaline earth metals and Cu(II) (Table 2).[43,45,46] Assuming that the material is poly-DHI implies that ca. 10−20% of the DHI molecules is complexed to metal. However, in the samples prepared in the presence of Fe(III), the metal content was approximately 20 atom %, which reflects the extremely high stability constants for Fe(III)-catecholates.[93] Iron forms 1:1, 1:2, and 1:3 complexes with the catechol moiety, depending on pH, but 1:1 complexes predominate at the synthesis pH. The rest of the iron coordination shell is filled by aqua ligands in this case, which form iron oxides upon dehydration in vacuum, and a high amount of iron was observed in the XPS images. Ce(IV) rapidly oxidizes catechol to *o*-quinone, and no complex formation is observed, while Fe(III), which is a significantly weaker oxidant under the synthesis conditions, was previously observed to form 1:1 catechol complexes.[39] No complex formation was observed with Cu(II).

In summary, the XPS study of the nanoparticles highlights two major differences between autoxidized polydopamine and material prepared using transition metals, a decreased nitrogen content, and various levels of metal in the material. However, because of the limited depth range of the method, both these results refer, strictly speaking, only to the surface region of the nanoparticles. In the surface region of a few nanometers, small nitrogen-rich molecules can diffuse out of particles and metal ions in material, whereas the core may be less affected. On the other hand, the core is formed from imbedded surface regions during the particle growth and the composition may have a complex dependence on the particle growth rate and material fluxes in and out.

CONCLUSIONS

Polydopamine nanoparticles formed by autoxidation and transition-metal-enhanced aerobic or anaerobic process were characterized. No significant differences were observed in the colloidal properties or UV−vis spectra of the nanoparticles prepared under different conditions. The nanoparticles possess ionizable groups on their surface, which affect their surface charge and solubilization in aqueous media. They cause a rapid increase in the nanoparticle dispersibility and a negative shift of the ζ potential in the pH range of 3−5, and both properties level off at higher pH. The transition pH range is in accordance with the pK_a values of the known dopamine decomposition species. In the case of metal oxidants, metals were found in the final materials also after thorough purification.

According to the XPS results, polydopamine prepared using transition metals is chemically superficially similar to the autoxidized material. The main difference is in the metal content, which is especially large in samples prepared using iron(III) as oxidant. The differences in the metal content can be rationalized by the redox and complexation properties of the metals using a simple general model presented. High metal content occurs with moderately oxidizing metals forming strong complexes with catecholate groups. In addition, metals seem to lead to a decrease in the nitrogen content in polydopamine. However, all of the samples display C−C, C−N/C−O, and C═O carbon species, and the pyrrolic nitrogen, attributed to intact dihydroxyindole moieties, is the major nitrogen species. Protonated free amino groups are also present, which implies incomplete five-ring closure. The XPS spectra also support the presence of carboxylic acid groups on the surface of the nanoparticles prepared under all conditions, in accordance with the dispersibility and ζ potential results. In addition, the shifts of the XPS spectra suggest that the cation−π interactions between the protonated free amino groups and the π-electron cloud of the dihydroxyindole moieties may be more pronounced in metal-induced polydopamine samples.

The study shows that the initial trends observed during the early stages of dopamine oxidation influence also the final product. All of the redox-active transition-metal oxidants studied can be used to rapidly prepare polydopamine under aerobic or anaerobic conditions, also in mildly acidic aqueous solutions, and at room temperature. However, the possible influence of the metal content, especially with iron-induced polydopamine nanoparticles, and the nitrogen loss should be taken into account.

ASSOCIATED CONTENT

Supporting Information

The Supporting Information is available free of charge on the ACS Publications website at DOI: 10.1021/acs.jpcb.8b11994.

UV−vis spectra of as-synthetized nanoparticles, an example of a nanoparticle dispersion at different pH values, SEM images of nanoparticles, AFM image of a polydopamine/PDADMA LbL multilayer, estimation of nanoparticle surface charge and coverage of ionized groups, literature compilation of XPS data for polydopamine, XPS peak binding energies and assignments, XPS survey spectra and Ce 3d, Fe 2p, and Cu $2p^3$ spectra of nanoparticles, and discussion of metal binding to polydopamine and author contributions (PDF)

AUTHOR INFORMATION

Corresponding Authors

*E-mails: mikko.salomaki@utu.fi (M.S.).
*E-mail: jukka.lukkari@utu.fi (J.L.).

DOI: 10.1021/acs.jpcb.8b11994
J. Phys. Chem. B 2019, 123, 2513−2524

ORCID

Mikko Salomäki: 0000-0001-6190-2073
Lauri Marttila: 0000-0002-8221-0954
Henri Kivelä: 0000-0003-1414-8893
Jukka Lukkari: 0000-0002-9409-7995

Notes

The authors declare no competing financial interest.

■ ACKNOWLEDGMENTS

T.O. gratefully acknowledges Suomen Kulttuurirahasto (Finnish Cultural Foundation, grant 00180808) and L.M. the Emil Aaltonen Foundation (grants 160165 N, 170166 N, and 180162 N) for a research grant.

■ REFERENCES

(1) Solano, F. Melanins: Skin Pigments and Much More—Types, Structural Models, Biological Functions, and Formation Routes. *New J. Sci.* **2014**, *2014*, 1−28.
(2) Simon, J. D.; Peles, D. N. The Red and the Black. *Acc. Chem. Res.* **2010**, *43*, 1452−1460.
(3) d'Ischia, M.; Wakamatsu, K.; Cicoira, F.; Di Mauro, E.; Garcia-Borron, J. C.; Commo, S.; Galván, I.; Ghanem, G.; Kenzo, K.; Meredith, P.; Pezzella, A.; Santato, C.; Sarna, T.; Simon, J. D.; Zecca, L.; Zucca, F. A.; Napolitano, A.; Ito, S. Melanins and Melanogenesis: From Pigment Cells to Human Health and Technological Applications. *Pigm. Cell Melanoma Res.* **2015**, *28*, 520−544.
(4) Meredith, P.; Sarna, T. The Physical and Chemical Properties of Eumelanin. *Pigm. Cell Melanoma Res.* **2006**, *19*, 572−594.
(5) Cicoira, F.; Santato, C.; Pezzella, A.; Wünsche, J. Eumelanin: An Old Natural Pigment and a New Material for Organic Electronics − Chemical, Physical, and Structural Properties in Relation to Potential Applications. In *Organic Electronics: Emerging Concepts and Technologies*; Cicoira, F., Santato, C., Eds.; Wiley-VCH Verlag GmbH & Co. KGaA, 2013; pp 113−137.
(6) Abbas, M.; D'Amico, F.; Morresi, L.; Pinto, N.; Ficcadenti, M.; Natali, R.; Ottaviano, L.; Passacantando, M.; Cuccioloni, M.; Angeletti, M.; Gunnella, R. Structural, Electrical, Electronic and Optical Properties of Melanin Films. *Eur. Phys. J. E* **2009**, *28*, 285−291.
(7) Raposo, G.; Marks, M. S. Melanosomes — Dark Organelles Enlighten Endosomal Membrane Transport. *Nat. Rev. Mol. Cell Biol.* **2007**, *8*, 786−797.
(8) Chang, L.; Chen, F.; Zhang, X.; Kuang, T.; Li, M.; Hu, J.; Shi, J.; Lee, L. J.; Cheng, H.; Li, Y. Synthetic Melanin E-Ink. *ACS Appl. Mater. Interfaces* **2017**, *9*, 16553−16560.
(9) Kim, Y. J.; Wu, W.; Chun, S.-E.; Whitacre, J. F.; Bettinger, C. J. Biologically Derived Melanin Electrodes in Aqueous Sodium-Ion Energy Storage Devices. *Proc. Natl. Acad. Sci. U.S.A.* **2013**, *110*, 20912−20917.
(10) Kim, Y. J.; Khetan, A.; Wu, W.; Chun, S.-E.; Viswanathan, V.; Whitacre, J. F.; Bettinger, C. J. Evidence of Porphyrin-Like Structures in Natural Melanin Pigments Using Electrochemical Fingerprinting. *Adv. Mater.* **2016**, *28*, 3173−3180.
(11) Lee, J.-W.; Cho, H.-B.; Nakayama, T.; Sekino, T.; Tanaka, S.-I.; Minato, K.; Ueno, T.; Suzuki, T.; Suematsu, H.; Tokoi, Y.; Niihara, K. Dye-Sensitized Solar Cells Using Purified Squid Ink Nanoparticles Coated on TiO_2 Nanotubes/nanoparticles. *J. Ceram. Soc. Jpn* **2013**, *121*, 123−127.
(12) Kim, D. J.; Ju, K.-Y.; Lee, J.-K. The Synthetic Melanin Nanoparticles Having an Excellent Binding Capacity of Heavy Metal Ions. *Bull. Korean Chem. Soc.* **2012**, *33*, 3788−3792.
(13) Ju, K.-Y.; Lee, Y.; Lee, S.; Park, S. B.; Lee, J.-K. Bioinspired Polymerization of Dopamine to Generate Melanin-Like Nanoparticles Having an Excellent Free-Radical-Scavenging Property. *Biomacromolecules* **2011**, *12*, 625−632.
(14) Rageh, M. M.; El-Gebaly, R. H.; Abou-Shady, H.; Amin, D. G. Melanin Nanoparticles (MNPs) Provide Protection against Whole-Body E-Irradiation Pound in Mice via Restoration of Hematopoietic Tissues. *Mol. Cell. Biochem.* **2015**, *399*, 59−69.
(15) Bao, X.; Zhao, J.; Sun, J.; Hu, M.; Yang, X. Polydopamine Nanoparticles as Efficient Scavengers for Reactive Oxygen Species in Periodontal Disease. *ACS Nano* **2018**, *12*, 8882−8892.
(16) Wu, T.-F.; Hong, J.-D. Dopamine-Melanin Nanofilms for Biomimetic Structural Coloration. *Biomacromolecules* **2015**, *16*, 660−666.
(17) Ball, V. Polydopamine Films and Particles with Catalytic Activity. *Catal. Today* **2018**, *301*, 196−203.
(18) Ho, C.-C.; Ding, S.-J. Structure, Properties and Applications of Mussel-Inspired Polydopamine. *J. Biomed. Nanotechnol.* **2014**, *10*, 3063−3084.
(19) Liu, M.; Zeng, G.; Wang, K.; Wan, Q.; Tao, L.; Zhang, X.; Wei, Y. Recent Developments in Polydopamine: An Emerging Soft Matter for Surface Modification and Biomedical Applications. *Nanoscale* **2016**, *8*, 16819−16840.
(20) Micillo, R.; Panzella, L.; Iacomino, M.; Prampolini, G.; Cacelli, I.; Ferretti, A.; Crescenzi, O.; Koike, K.; Napolitano, A.; d'Ischia, M. Eumelanin Broadband Absorption Develops from Aggregation-Modulated Chromophore Interactions under Structural and Redox Control. *Sci. Rep.* **2017**, *7*, No. 41532.
(21) Liebscher, J.; Mrówczynski, R.; Scheidt, H. A.; Filip, C.; Hadade, N. D.; Turcu, R.; Bende, A.; Beck, S. Structure of Polydopamine: A Never-Ending Story? *Langmuir* **2013**, *29*, 10539−10548.
(22) d'Ischia, M.; Napolitano, A.; Ball, V.; Chen, C.-T.; Buehler, M. J. Polydopamine and Eumelanin: From Structure−Property Relationships to a Unified Tailoring Strategy. *Acc. Chem. Res.* **2014**, *47*, 3541−3550.
(23) Liu, Y.; Ai, K.; Lu, L. Polydopamine and Its Derivative Materials: Synthesis and Promising Applications in Energy, Environmental, and Biomedical Fields. *Chem. Rev.* **2014**, *114*, 5057−5115.
(24) Okuda, H.; Yoshino, K.; Wakamatsu, K.; Ito, S.; Sota, T. Degree of Polymerization of 5,6-dihydroxyindole-derived Eumelanin from Chemical Degradation Study. *Pigm. Cell Melanoma Res.* **2014**, *27*, 664−667.
(25) Della Vecchia, N. F.; Avolio, R.; Alfè, M.; Errico, M. E.; Napolitano, A.; d'Ischia, M. Building-Block Diversity in Polydopamine Underpins a Multifunctional Eumelanin-Type Platform Tunable Through a Quinone Control Point. *Adv. Funct. Mater.* **2013**, *23*, 1331−1340.
(26) Hong, S.; Wang, Y.; Park, S. Y.; Lee, H. Progressive Fuzzy Cation-Π Assembly of Biological Catecholamines. *Sci. Adv.* **2018**, *4*, No. eaat7457.
(27) Chen, C.-T.; Ball, V.; de Almeida Gracio, J. J.; Singh, M. K.; Toniazzo, V.; Ruch, D.; Buehler, M. J. Self-Assembly of Tetramers of 5, 6-Dihydroxyindole Explains the Primary Physical Properties of Eumelanin: Experiment, Simulation, and Design. *ACS Nano* **2013**, *7*, 1524−1532.
(28) Kim, Y. J.; Khetan, A.; Wu, W.; Chun, S.-E.; Viswanathan, V.; Whitacre, J. F.; Bettinger, C. J. Evidence of Porphyrin-Like Structures in Natural Melanin Pigments Using Electrochemical Fingerprinting. *Adv. Mater.* **2016**, *28*, 3173−3180.
(29) Alfieri, M. L.; Micillo, R.; Panzella, L.; Crescenzi, O.; Oscurato, S. L.; Maddalena, P.; Napolitano, A.; Ball, V.; d'Ischia, M. Structural Basis of Polydopamine Film Formation: Probing 5,6-Dihydroxyindole-Based Eumelanin Type Units and the Porphyrin Issue. *ACS Appl. Mater. Interfaces* **2017**, 7670.
(30) Mondal, S.; Thampi, A.; Puranik, M. Kinetics of Melanin Polymerization during Enzymatic and Nonenzymatic Oxidation. *J. Phys. Chem. B* **2018**, *122*, 2047−2063.
(31) Yu, X.; Fan, H.; Liu, Y.; Shi, Z.; Jin, Z. Characterization of Carbonized Polydopamine Nanoparticles Suggests Ordered Supramolecular Structure of Polydopamine. *Langmuir* **2014**, *30*, 5497−5505.
(32) Jin, Z.; Fan, H. The Modulation of Melanin-like Materials: Methods, Characterization and Applications. *Polym. Int.* **2016**, *65*, 1258−1266.

DOI: 10.1021/acs.jpcb.8b11994
J. Phys. Chem. B 2019, 123, 2513−2524

(33) Belitsky, J. M.; Ellowitz, M. Z.; Lye, D.; Kilbo, A. L. Small Molecule Modulators of Aggregation in Synthetic Melanin Polymerizations. *Bioorg. Med. Chem. Lett.* **2012**, *22*, 5503−5507.
(34) Lee, H.; Dellatore, S. M.; Miller, W. M.; Messersmith, P. B. Mussel-Inspired Surface Chemistry for Multifunctional Coatings. *Science* **2007**, *318*, 426−430.
(35) Strube, O. I.; Büngeler, A.; Bremser, W. Site-Specific In Situ Synthesis of Eumelanin Nanoparticles by an Enzymatic Autodeposition-Like Process. *Biomacromolecules* **2015**, *16*, 1608−1613.
(36) Della Vecchia, N. F.; Cerruti, P.; Gentile, G.; Errico, M. E.; Ambrogi, V.; d'Errico, G.; Longobardi, S.; Napolitano, A.; Paduano, L.; Carfagna, C.; d'Ischia, M. Artificial Biomelanin: Highly Light-Absorbing Nano-Sized Eumelanin by Biomimetic Synthesis in Chicken Egg White. *Biomacromolecules* **2014**, *15*, 3811−3816.
(37) Bergtold, C.; Hauser, D.; Chaumont, A.; Yakhlifi, S. E.; Mateescu, M.; Meyer, F.; Metz-Boutigue, M.-H.; Frisch, B.; Schaaf, P.; Ihiawakrim, D.; Ersen, O.; Monnier, C. A.; Petri-Fink, A.; Rothen-Rutishauser, B.; Ball, V. Mimicking the Chemistry of Natural Eumelanin Synthesis: The KE Sequence in Polypeptides and in Proteins Allows for a Specific Control of Nanosized Functional Polydopamine Formation. *Biomacromolecules* **2018**, *19*, 3693−3704.
(38) Mateescu, M.; Metz-Boutigue, M.-H.; Bertani, P.; Ball, V. Polyelectrolytes to Produce Nanosized Polydopamine. *J. Colloid Interface Sci.* **2016**, *469*, 184−190.
(39) Salomäki, M.; Marttila, L.; Kivelä, H.; Ouvinen, T.; Lukkari, J. Effects of pH and Oxidants on the First Steps of Polydopamine Formation: A Thermodynamic Approach. *J. Phys. Chem. B* **2018**, *122*, 6314−6327.
(40) Zheng, W.; Fan, H.; Wang, L.; Jin, Z. Oxidative Self-Polymerization of Dopamine in an Acidic Environment. *Langmuir* **2015**, *31*, 11671−11677.
(41) Wei, Q.; Zhang, F.; Li, J.; Li, B.; Zhao, C. Oxidant-Induced Dopamine Polymerization for Multifunctional Coatings. *Polym. Chem* **2010**, *1*, 1430−1433.
(42) Ponzio, F.; Barthès, J.; Bour, J.; Michel, M.; Bertani, P.; Hemmerlé, J.; d'Ischia, M.; Ball, V. Oxidant Control of Polydopamine Surface Chemistry in Acids: A Mechanism-Based Entry to Superhydrophilic-Superoleophobic Coatings. *Chem. Mater.* **2016**, *28*, 4697−4705.
(43) Han, X.; Tang, F.; Jin, Z. Free-Standing Polydopamine Films Generated in the Presence of Different Metallic Ions: The Comparison of Reaction Process and Film Properties. *RSC Adv.* **2018**, *8*, 18347−18354.
(44) Jiao, L.; Xu, Z.; Du, W.; Li, H.; Yin, M. Fast Preparation of Polydopamine Nanoparticles Catalyzed by Fe^{2+}/H_2O_2 for Visible Sensitive Smartphone-Enabled Cytosensing. *ACS Appl. Mater. Interfaces* **2017**, *9*, 28339−28345.
(45) Bernsmann, F.; Ball, V.; Addiego, F.; Ponche, A.; Michel, M.; de Almeida Gracio, J. J.; Toniazzo, V.; Ruch, D. Dopamine−Melanin Film Deposition Depends on the Used Oxidant and Buffer Solution. *Langmuir* **2011**, *27*, 2819−2825.
(46) Ball, V.; Gracio, J.; Vila, M.; Singh, M. K.; Metz-Boutigue, M.-H.; Michel, M.; Bour, J.; Toniazzo, V.; Ruch, D.; Buehler, M. J. Comparison of Synthetic Dopamine-Eumelanin Formed in the Presence of Oxygen and Cu^{2+} Cations as Oxidants. *Langmuir* **2013**, *29*, 12754−12761.
(47) Krumova, K.; Cosa, G. Overview of Reactive Oxygen Species. In *Singlet Oxygen: Applications in Biosciences and Nanosciences*; Nonell, S., Flors, C., Eds.; Royal Society of Chemistry, 2016; Vol. *1*, pp 1−21.
(48) Valentine, J. S. Dioxygen Reactions. In *Bioinorganic Chemistry*; Bertini, I., Gray, H. B., Lippard, S. J., Valentine, J. S., Eds.; University Science Books, 1994; pp 253−313.
(49) Szpoganicz, B.; Gidanian, S.; Kong, P.; Farmer, P. Metal Binding by Melanins: Studies of Colloidal Dihydroxyindole-Melanin, and Its Complexation by Cu (II) and Zn (II) Ions. *J. Inorg. Biochem.* **2002**, *89*, 45−53.
(50) Bisaglia, M.; Mammi, S.; Bubacco, L. Kinetic and Structural Analysis of the Early Oxidation Products of Dopamine: Analysis of the Interactions with α-Synuclein. *J. Biol. Chem.* **2007**, *282*, 15597−15605.
(51) Koval, I. A.; Gamez, P.; Belle, C.; Selmeczi, K.; Reedijk, J. Synthetic Models of the Active Site of Catechol Oxidase: Mechanistic Studies. *Chem. Soc. Rev.* **2006**, *35*, 814−840.
(52) Schweitzer, G. K.; Pesterfield, L. L. *The Aqueous Chemistry of the Elements*; Oxford University Press, 2010.
(53) Weidman, S. W.; Kaiser, E. T. The Mechanism of the Periodate Oxidation of Aromatic Systems. III. A Kinetic Study of the Periodate Oxidation of Catechol. *J. Am. Chem. Soc.* **1966**, *88*, 5820−5827.
(54) Ju, K.-Y.; Lee, J. W.; Im, G. H.; Lee, S.; Pyo, J.; Park, S. B.; Lee, J. H.; Lee, J.-K. Bio-Inspired, Melanin-like Nanoparticles as a Highly Efficient Contrast Agent for T1-Weighted Magnetic Resonance Imaging. *Biomacromolecules* **2013**, *14*, 3491−3497.
(55) Salomäki, M.; Tupala, M.; Parviainen, T.; Leiro, J.; Karonen, M.; Lukkari, J. Preparation of Thin Melanin-Type Films by Surface-Controlled Oxidation. *Langmuir* **2016**, *32*, 4103−4112.
(56) Butt, H.-J.; Kappl, M. *Surface and Interfacial Forces*; Wiley-VCH: Weinheim, Germany, 2009.
(57) Martin, R. B. Zwitterion Formation Upton Deprotonation in L-3,4-Dihydroxyphenylalanine and Other Phenolic Amines. *J. Phys. Chem.* **1971**, *75*, 2657−2661.
(58) Jastrzebski, R.; Weckhuysen, B. M.; Bruijnincx, P. C. A. Catalytic Oxidative Cleavage of Catechol by a Non-Heme Iron(III) Complex as a Green Route to Dimethyl Adipate. *Chem. Commun.* **2013**, *49*, 6912.
(59) Carraher, J. M.; Pfennig, T.; Rao, R. G.; Shanks, B. H.; Tessonnier, J.-P. *cis,cis*-Muconic Acid Isomerization and Catalytic Conversion to Biobased Cyclic-C6-1,4-Diacid Monomers. *Green Chem.* **2017**, *19*, 3042−3050.
(60) Jalil, A. H.; Pyell, U. Quantification of Zeta-Potential and Electrokinetic Surface Charge Density for Colloidal Silica Nanoparticles Dependent on Type and Concentration of the Counterion: Probing the Outer Helmholtz Plane. *J. Phys. Chem. C* **2018**, *122*, 4437−4453.
(61) Ball, V. Determination of the Extinction Coefficient of "polydopamine" Films Obtained by Using $NaIO_4$ as the Oxidant. *Mater. Chem. Phys.* **2017**, *186*, 546−551.
(62) Bernsmann, F.; Ersen, O.; Voegel, J.; Jan, E.; Kotov, N. A.; Ball, V. Melanin-Containing Films: Growth from Dopamine Solutions versus Layer-by-Layer Deposition. *ChemPhysChem* **2010**, *11*, 3299−3305.
(63) Seah, M. P. Simple Universal Curve for the Energy-Dependent Electron Attenuation Length for All Materials. *Surf. Interface Anal.* **2012**, *44*, 1353−1359.
(64) Yamahara, R.; Ogo, S.; Masuda, H.; Watanabe, Y. (Catecholato)iron(III) Complexes: Structural and Functional Models for the Catechol-Bound iron(III) Form of Catechol Dioxygenases. *J. Inorg. Biochem.* **2002**, *88*, 284−294.
(65) Stepanović, S.; Angelone, D.; Gruden, M.; Swart, M. The Role of Spin States in the Catalytic Mechanism of the Intra- and Extradiol Cleavage of Catechols by O_2. *Org. Biomol. Chem.* **2017**, *15*, 7860−7868.
(66) Ding, Y.; Weng, L.-T.; Yang, M.; Yang, Z.; Lu, X.; Huang, N.; Leng, Y. Insights into the Aggregation/Deposition and Structure of a Polydopamine Film. *Langmuir* **2014**, *30*, 12258−12269.
(67) Zangmeister, R. A.; Morris, T. A.; Tarlov, M. J. Characterization of Polydopamine Thin Films Deposited at Short Times by Autoxidation of Dopamine. *Langmuir* **2013**, *29*, 8619−8628.
(68) Coskun, H.; Aljabour, A.; Luna, P. D.; Farka, D.; Greunz, T.; Stifter, D.; Kus, M.; Zheng, X.; Liu, M.; Hassel, A. W.; Schöfberger, W.; Sargent, E. H.; Sariciftci, N. S.; Stadler, P. Biofunctionalized Conductive Polymers Enable Efficient CO_2 Electroreduction. *Sci. Adv.* **2017**, *3*, No. e1700686.
(69) Wang, Z.; Tang, F.; Fan, H.; Wang, L.; Jin, Z. Polydopamine Generates Hydroxyl Free Radicals under Ultraviolet-Light Illumination. *Langmuir* **2017**, *33*, 5938−5946.
(70) Bernsmann, F.; Ponche, A.; Ringwald, C.; Hemmerlé, J.; Raya, J.; Bechinger, B.; Voegel, J.-C.; Schaaf, P.; Ball, V. Characterization of

DOI: 10.1021/acs.jpcb.8b11994
J. Phys. Chem. B 2019, 123, 2513−2524

Dopamine-Melanin Growth on Silicon Oxide. *J. Phys. Chem. C* **2009**, *113*, 8234−8242.
(71) Xi, Z.-Y.; Xu, Y.-Y.; Zhu, L.-P.; Wang, Y.; Zhu, B.-K. A Facile Method of Surface Modification for Hydrophobic Polymer Membranes Based on the Adhesive Behavior of poly(DOPA) and Poly(dopamine). *J. Membr. Sci.* **2009**, *327*, 244−253.
(72) Chao, C.; Liu, J.; Wang, J.; Zhang, Y.; Zhang, B.; Zhang, Y.; Xiang, X.; Chen, R. Surface Modification of Halloysite Nanotubes with Dopamine for Enzyme Immobilization. *ACS Appl. Mater. Interfaces* **2013**, *5*, 10559−10564.
(73) Yamashita, T.; Hayes, P. Analysis of XPS Spectra of Fe^{2+} and Fe^{3+} Ions in Oxide Materials. *Appl. Surf. Sci.* **2008**, *254*, 2441−2449.
(74) Filippidi, E.; Cristiani, T. R.; Eisenbach, C. D.; Waite, J. H.; Israelachvili, J. N.; Ahn, B. K.; Valentine, M. T. Toughening Elastomers Using Mussel-Inspired Iron-Catechol Complexes. *Science* **2017**, *358*, 502−505.
(75) Susi, T.; Pichler, T.; Ayala, P. X-Ray Photoelectron Spectroscopy of Graphitic Carbon Nanomaterials Doped with Heteroatoms. *Beilstein J. Nanotechnol.* **2015**, *6*, 177−192.
(76) Jiang, Z.; Jiang, Z.; Tian, X.; Chen, W. Amine-Functionalized Holey Graphene as a Highly Active Metal-Free Catalyst for the Oxygen Reduction Reaction. *J. Mater. Chem. A* **2014**, *2*, 441−450.
(77) Dietrich, P. M.; Graf, N.; Gross, T.; Lippitz, A.; Krakert, S.; Schüpbach, B.; Terfort, A.; Unger, W. E. S. Amine Species on Self-assembled Monolayers of ω-aminothiolates on Gold as Identified by XPS and NEXAFS Spectroscopy. *Surf. Interface Anal.* **2010**, *42*, 1184−1187.
(78) Lukkari, J.; Kleemola, K.; Meretoja, M.; Ollonqvist, T.; Kankare, J. Electrochemical Post-Self-Assembly Transformation of 4-Aminothiophenol Monolayers on Gold Electrodes. *Langmuir* **1998**, *14*, 1705−1715.
(79) Ryu, S.; Chou, J. B.; Lee, K.; Lee, D.; Hong, S. H.; Zhao, R.; Lee, H.; Kim, S. Direct Insulation-to-Conduction Transformation of Adhesive Catecholamine for Simultaneous Increases of Electrical Conductivity and Mechanical Strength of CNT Fibers. *Adv. Mater.* **2015**, *27*, 3250−3255.
(80) Kim, Y. J.; Wu, W.; Chun, S.-E.; Whitacre, J. F.; Bettinger, C. J. Biologically Derived Melanin Electrodes in Aqueous Sodium-Ion Energy Storage Devices. *Proc. Natl. Acad. Sci. U.S.A.* **2013**, *110*, 20912−20917.
(81) Il'ichev, Y. V.; Simon, J. D. Building Blocks of Eumelanin: Relative Stability and Excitation Energies of Tautomers of 5,6-Dihydroxyindole and 5,6-Indolequinone. *J. Phys. Chem. B* **2003**, *107*, 7162−7171.
(82) d'Ischia, M.; Napolitano, A.; Pezzella, A. 5,6-Dihydroxyindole Chemistry: Unexplored Opportunities Beyond Eumelanin. *Eur. J. Org. Chem.* **2011**, *2011*, 5501−5516.
(83) Hong, L.; Simon, J. D. Current Understanding of the Binding Sites, Capacity, Affinity, and Biological Significance of Metals in Melanin. *J. Phys. Chem. B* **2007**, *111*, 7938−7947.
(84) Abu-Husein, T.; Schuster, S.; Egger, D. A.; Kind, M.; Santowski, T.; Wiesner, A.; Chiechi, R.; Zojer, E.; Terfort, A.; Zharnikov, M. The Effects of Embedded Dipoles in Aromatic Self-Assembled Monolayers. *Adv. Funct. Mater.* **2015**, *25*, 3943−3957.
(85) Taucher, T. C.; Hehn, I.; Hofmann, O. T.; Zharnikov, M.; Zojer, E. Understanding Chemical versus Electrostatic Shifts in X-Ray Photoelectron Spectra of Organic Self-Assembled Monolayers. *J. Phys. Chem. C* **2016**, *120*, 3428−3437.
(86) Salomäki, M.; Räsänen, M.; Leiro, J.; Huti, T.; Tenho, M.; Lukkari, J.; Kankare, J. Oxidative Inorganic Multilayers for Polypyrrole Film Generation. *Adv. Funct. Mater.* **2010**, *20*, 2140−2147.
(87) Bêche, E.; Charvin, P.; Perarnau, D.; Abanades, S.; Flamant, G. Ce 3d XPS Investigation of Cerium Oxides and Mixed Cerium Oxide ($Ce_xTi_yO_z$). *Surf. Interface Anal.* **2008**, *40*, 264−267.
(88) Kawatsura, K.; Takeshima, N.; Imaoku, T.; Takahiro, K.; Mokuno, Y.; Horino, Y.; Sekioka, T.; Terasawa, M. High-Resolution X-Ray Spectroscopy for Copper and Copper Oxides and a New WDX System Using an Ion Microbeam. *Nucl. Instrum. Methods Phys. Res., Sect. B* **2002**, *193*, 877−882.
(89) Sakai, Y.; Ninomiya, S.; Hiraoka, K. XPS Depth Analysis of CuO by Electrospray Droplet Impact. *Surf. Interface Anal.* **2012**, *44*, 938−941.
(90) d'Ischia, M.; Napolitano, A.; Pezzella, A.; Land, E. J.; Ramsden, C. A.; Riley, P. A. 5,6-Dihydroxyindoles and Indole-5,6-Diones. In *Advances in Heterocyclic Chemistry*; Katritzky, A., Ed.; Elsevier, 2005; Vol. *89*, pp 1−63.
(91) Kumar, T. N.; Sivabalan, S.; Chandrasekaran, N.; Phani, K. L. N. Ferrocene-Functionalized Polydopamine as a Novel Redox Matrix for H_2O_2 Oxidation. *J. Mater. Chem. B* **2014**, *2*, 6081−6088.
(92) Sucha, L.; Kotrlý, S. *Solution Equilibria in Analytical Chemistry*; van Nostrand Reinhold: London, 1972.
(93) Holten-Andersen, N.; Harrington, M. J.; Birkedal, H.; Lee, B. P.; Messersmith, P. B.; Lee, K. Y. C.; Waite, J. H. pH-Induced Metal-Ligand Cross-Links Inspired by Mussel Yield Self-Healing Polymer Networks with near-Covalent Elastic Moduli. *Proc. Natl. Acad. Sci. U.S.A.* **2011**, *108*, 2651−2655.
(94) Sun, Y.; Pham, A. N.; Waite, T. D. Elucidation of the Interplay between Fe(II), Fe(III), and Dopamine with Relevance to Iron Solubilization and Reactive Oxygen Species Generation by Catecholamines. *J. Neurochem.* **2016**, *137*, 955−968.
(95) Jameson, R. F.; Wilson, M. F. Thermodynamics of the Interactions of Catechol with Transition Metals. Part II. Copper and Nickel Complexes of Catechol. *J. Chem. Soc., Dalton Trans.* **1972**, 2614−2616.
(96) Buchanan, R. M.; Wilson-Blumenberg, C.; Trapp, C.; Larsen, S. K.; Greene, D. L.; Pierpont, C. G. Counter Ligand Dependence of Charge Distribution in Copper-Quinone Complexes. Structural and Magnetic Properties of (3,5-Di-Tert-butylcatecholato)(bipyridine)-copper(II). *Inorg. Chem.* **1986**, *25*, 3070−3076.
(97) Zucca, F. A.; Segura-Aguilar, J.; Ferrari, E.; Muñoz, P.; Paris, I.; Sulzer, D.; Sarna, T.; Casella, L.; Zecca, L. Interactions of Iron, Dopamine and Neuromelanin Pathways in Brain Aging and Parkinson's Disease. *Prog. Neurobiol.* **2017**, *155*, 96−119.

DOI: 10.1021/acs.jpcb.8b11994
J. Phys. Chem. B 2019, 123, 2513−2524